RSC Advances

ROYAL SOCIETY OF CHEMISTRY

www.rsc.org/advances

Direct templating assembly route for preparation of highly-dispersed vanadia species encapsulated in mesoporous MCM-41 channel

Fu yang, Shuying Gao, Cuirong Xiong, Saifu Long, Xiaoming Li, Tao Xi, Yan Kong*

State Key Laboratory of Materials-Oriented Chemical Engineering, Nanjing Tech University, Nanjing 210009, China

Corresponding Author.

*Email: kongy36@njtech.edu.cn. Tel & Fax: 86-025-83587860.

Abstract: The statues of active sites such as number and dispersion on the surface of support are

essential to improve the catalytic activity. In this paper, highly-dispersed and controllable quantities of vanadia species within channel of mesoporous MCM-41 were directly prepared by a direct templating assembly method ($S^+L^-M^+I^-$). This method was based on the self-assembly of cationic surfactants (CTA^+, S^+), chelating agents (citrate ions, L^-), vanadyl ions (VO^{2+}, M^+) and silicates oligomers (I^-) by the electrostatic and chelating interaction. First, the citrate ions were absorbed on the CTA^+ micelles' surface by electrostatic interaction, the vanadyl ions subsequently were anchored on their surface by chelating with citrate ions to form metallomicelles. Finally, the silicates were deposited on the metallomicelles to obtain the targeted product. The structure of samples, especially the oxidation state and surface distribution of vanadium species on the mesoporous silica were efficiently characterized with different techniques including XRD, N_2 adsorption, SEM, TEM, UV-vis, XPS, FT-IR, ICP and H_2-TPR. Furthermore, the obtained samples, using hydroxylation of benzene as a probe reaction, exhibited superior catalytic activities when compared with post-synthesized sample.

Keywords: Templating Assembly, Highly-dispersed, Vanadia Species, Encapsulation, MCM-41

1. Introduction

Mesoporous silica materials are well-known as a good carrier for their oriented-ordered nanochannels and large surface areas,[1-7] which have been widely researched with functional modifications over the past two decades.[8-14] A series of derived mesoporous composites have also shown potential applications in biomedical science,[15] optical sensing,[16] catalysis,[17-19] etc.

Supported vanadium oxide catalysts contain vanadium oxide phase deposited on mesoporous silica and have found extensive applications as oxidation catalysts in the chemical and petroleum industries. .In particular, supported vanadia phase presented as surface vanadium oxide species is responsible for the overall catalytic activity and selectivity.[20] In addition, quantized catalytic active centers such as particles or clusters would be preferable to enhance catalytic activities in catalytic process. Therefore, the dispersion and number of the catalytic active sites on the supports would be the key factors influencing catalytic activities for the catalysts. Many synthesis methods including sorption, phase transitions, ion exchange, complexation and covalent grafting have been utilized to modify mesoporous silica for the preparation of the catalytic materials functionalized with metal species. [21-26]

These methods, however, require multistep synthesis processes and a large number of raw materials' modifying works,[27-30] resulting in destruction of the material's structure and regularity. Moreover, the precursors tend to be absorbed on the external surface of mesoporous silica, leading to large particles growing outside the mesopores.[31] It was therefore highly desirable in this current study to seek a direct synthetic route for obtaining functional catalytic material with high-dispersion and high-loading catalytic active sites.

Herein, we have therefore attempted to develop a simple and efficient templating synthetic method ($S^+L^-M^+I^-$) for modification of micelles to directly obtain surface-functional mesoporous silica with highly-dispersed and controllable quantities of vanadia species. We, though this method, prepared the metallomicelles ($S^+L^-M^+$) with metal complexes attached on their surface by self-assembly of CTA^+

(S^+), citrate (L^-) and VO^{2+} (M^+) ions. We subsequently used them to synthesize our targeted mesoporous composites. In addition, different characterization methods were applied to test materials' structure and oxidation state and distribution of vanadium oxides. Finally, benzene hydroxylation was employed as a probe reaction to evaluate catalytic activities of the resultant samples.

2. Experimental section

2.1 Materials

Cetyltrimethylammonium bromide (CTAB, 99%), vanadyl sulfate ($VOSO_4$, AR), vanadyl acetylacetonate ($C_{10}H_{14}O_5V$, AR), tetraethylorthosilicate (TEOS, AR), acetone (AR), sodium citrate (AR), ammonia solution (25 wt%), acetonitrile (AR) and benzene (AR) were obtained from Sinopharm Chemical Reagent Co., Ltd. Hydrogen peroxide (H_2O_2, 30 wt%) was purchased from Shanghai Chemical Corporation Pilot.

2.2. Preparation of V/MCM mesoporous composites

Typical synthesized process contained four facile procedures of mixing of surfactants, metallization of micelles, coating of silicates and calcination. A specific preparation process was as follows: 3.644 g CTAB (0.01 mol) were dissolved in 200 mL distilled water. Vanadium amount in composites was adjusted by controlling molar ratio (VO^{2+}/CTA^+=0.2, 0.3, 0.4, 0.5, 0.6). Before adding $VOSO_4$, equimolar amount sodium citrate were added into CTAB solutions, and then different amounts of $VOSO_4$ were added respectively in above mixed solutions with an additional stirring for 30 min. The pH of the resulting solutions were adjusted to 10 with concentrated ammonia (25 wt %), subsequently, 11.15 mL of TEOS was rapidly added and stirred for 1 h under strong agitation. The obtained gel was then transferred to Teflon stainless autoclave and aged at 100 °C for 3 days. The resulting samples were centrifuged and washed with distilled water and ethanol three times respectively. Finally, the obtained dried samples were calcined at 550 °C for 5 h in dry air stream with a heating rate of 1 °Cmin^{-1}. The

calcined samples were designated as x V/MCM (where x was 100 times of V/CTAB molar ratio).

By contrast, another MCM-supported vanadia catalysts were prepared by typical wet impregnation method. Briefly, pure MCM-41 carrier (0.15 g) was evenly dispersed in an ethanolic solution containing 0.074 g of vanadyl acetylacetonate (0.28 mmol) by ultrasonic treatment and the ethanol was rota evaporated until complete dryness. The catalysts were then dried in air at 100°C overnight and then calcined at 550°C for 6 h in air, to obtain 60V/MCM sample (calculated molar ratio V/Si=11.2%).

2.3. Characterization

The XRD patterns of the samples were collected with Smartlab TM 9 KW (Rigaku Corporation, Tokyo, Japan) equipped with a rotating anode and Cu Kα radiation (λ = 0.154178 nm).

The N_2 (77.4 K) adsorption-desorption measurements were carried out with BELSORP-MINI volumetric adsorption analyzer (BEL Japan, Osaka, Japan) in a relative pressure range P/P_0 from 0.01 to 0.99. The annealed samples were outgassed in vacuum at 150 °C for 5 h and before measurements. The specific surface areas and distribution of pore size were calculated using the Brunauer-Emmet-Teller (BET) and Barrett-Joyner-Halenda (BJH) methods, respectively.

High-resolution transmission electron microscopy (HRTEM) images were recorded on a JEM-2010 EX microscope (JEOL, Tokyo, Japan), which was operated at an accelerating voltage of 200 kV. The samples were crushed in A.R. grade ethanol and the resulting suspension was allowed to dry on carbon film supported on copper grids.

Diffused Reflection UV-Vis spectra of samples were obtained in the range of 200-800 nm by Lambda 950 spectrophotometer (PerkinElmer, Waltham, MA, USA).

The X-ray photoelectron spectra (XPS) were performed on a PHI 5000 Versa Probe X-ray photoelectron spectrometer (ULVAC-PHI, Kanagawa, Japan) equipped with Al K_α radiation (1486.6 eV). The C1s peak at 284.6 eV was used as the reference for binding energy.

Fourier Transform Infrared (FT-IR) spectra from the samples were obtained in the range of

400-4000 cm^{-1}, with powders dispersed on the KBr on Bruker VECTOR22 resolution (Bruker, Bruker, Germany).

The vanadium content in the samples were determined using a PE Optima 2000DV (PerkinElmer, Waltham, MA, USA) Inductively Coupling Plasma emission spectrometer (ICP). The samples were completely dissolved in hydrofluoric acid before analysis.

Hydrogen temperature programmed reduction (H_2-TPR) measurements were performed utilizing a fixed-bed reactor under a flow of 10 % H_2/Ar gas mixture and a heating rate of 10 ℃ /min from room temperature to 750 °C. Before the TPR analysis, the carbonates and hydrates impurities were removed by flowing argon over the catalyst at a flow rate of 30 mL/min at 300 °C for 1 h and the system was then cooled to room temperature. The amount of H_2 uptake during the reduction was measured continuously using a thermal conductivity detector (TCD).

2.4. Catalysis performance tests

The catalytic activity assessment of the V/MCM on direct oxidation of benzene was performed as follows: 0.1 g catalyst, 2 mL benzene and 6.89 mL H_2O_2 were all added into a 50 mL flask containing 15 mL acetonitrile. The mixed solutions system was then stirred for 10 h at 30 °C water bath. The products from the reactions were finally analyzed by a SP-6890 gas chromatograph (Lunan Ruihong Chemical Instrument Co. LTD, China) with 0.32 mm × 30 m SE-54 capillary column. The conversion and selectivity of products were calculated by external standard method.

In order to investigate the recycling properties of the directly synthesized and post-synthesized catalysts, the two solid catalysts were separated from the reaction mixture by centrifugation and used again in a fresh reaction respectively.

3. Results and discussion

The electrostatic assembly approach has been proposed for synthesis of MCM-41.[32] The primary

pathway involved the direct co-condensation of anionic inorganic species (I^-), with a cationic surfactant (S^+) corresponding to assembled ion pairs from a type S^+I^-. In this study, chelating agents (citrate ions) and metal cations (VO^{2+}) were introduced to cooperatively assemble with cationic surfactant and anionic inorganic species by electrostatic and chelating interaction.

The scheme 1 illustrates the synthetic mechanism, the raw micelles were consisted of CTA^+, whose tail carrying electropositive ions would spontaneously absorb the citrate ions (L^-) with negative charge. The added metal ions VO^{2+} would then coordinate with citrate ions on the micelles surface to form the metallomicelles. Finally, deposition of silicate oligomers on the surface of the micelles would lead to formation of vanadium functional mesocomposites.

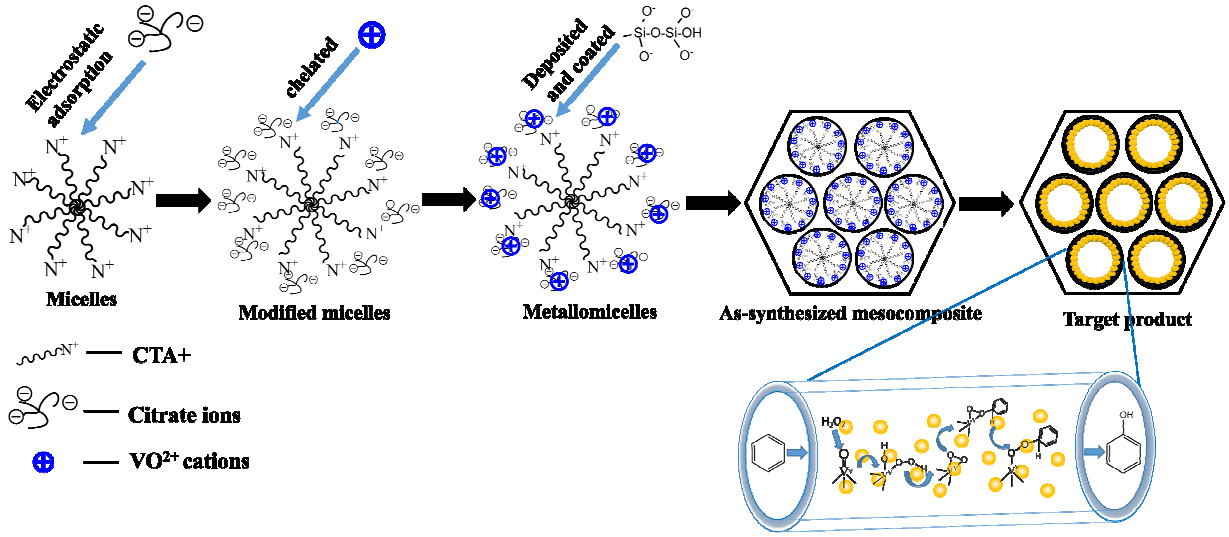

Scheme 1. Mechanism for material self-assembly

3.1 Characterizations of mesocomposites' structure

The structural characteristics of all the samples were evaluated by low-angle XRD analysis (Fig. 1), N_2 absorption/desorption measurements (Fig. 2) and TEM (Fig. 3). As shown in Fig. 1, all the prepared samples exhibited a strong (100) diffraction peak at $2\theta \approx$ 2-3°, indicating the mesoporous structure of the samples. In addition, the presence of two relatively weak, 110 and 200 diffraction peaks at $2\theta \approx$ 3-5°, suggested highly ordered two-dimensional (*2D*) hexagonal structure with a p6mm symmetry, which was

typical for the MCM-41 mesoporous materials. These observations revealed that the highly ordered mesoporous structures of the host materials have been retained, even vanadium oxides were encapsulated inside their matrices. Meanwhile, three typical characteristic peaks (100), (110) and (200) showed gradual shift to the small angle with increasing vanadium contents in samples, indicating the increase of d_{100} interplanar spacing. This finding may be associated with the enlargement of metallomicelles by the coordination with increasing vanadyl ions.

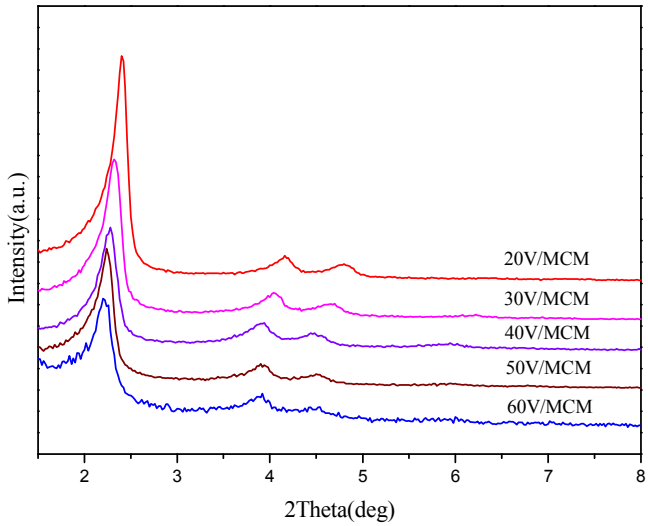

Fig. 1 Low-angle XRD patterns of samples containing different vanadium contents.

N_2 adsorption/desorption isotherms (Fig. 2) showed that all the samples had typical type IV characteristics curve with a H1 type hysteresis loop, indicating that the synthesized samples were mesoporous materials with two-dimensional hexagonal structure. Also, more vanadium oxides were incorporated inside the MCM-41 and the type IV shape was still maintained, suggesting the remained ordered mesoporous structure. On the other hand, the separation spacing of adsorption and desorption isotherms between relative pressure (P/P_0) 0.5 and 0.9 exhibited an increasing trend with increasing vanadium loading in samples. This phenomenon could be attributed to increasing stacking pore between particles due to decreasing size of particles with increasing vanadium loading, which was in accordance with SEM results. The more detailed structural characteristics of the samples are further summarized in

Table 1. When we compared the pore size of different samples, we observed a gradually increasing trend of pore diameter with increasing vanadium amounts. This result may be associated with the fact that increasing amounts of metal complexes were adsorbed on the surface of the micelles, leading to larger sizes of the metallomicelles. In addition, it is worth noting that pore wall thickness (d_w) increased from 1.69 nm to 1.96 nm with increasing vanadium amounts in the samples. We suggested that the increasing thickness could be assigned to vanadium oxides layer loaded on the mesoporous silica MCM-41 pore walls.

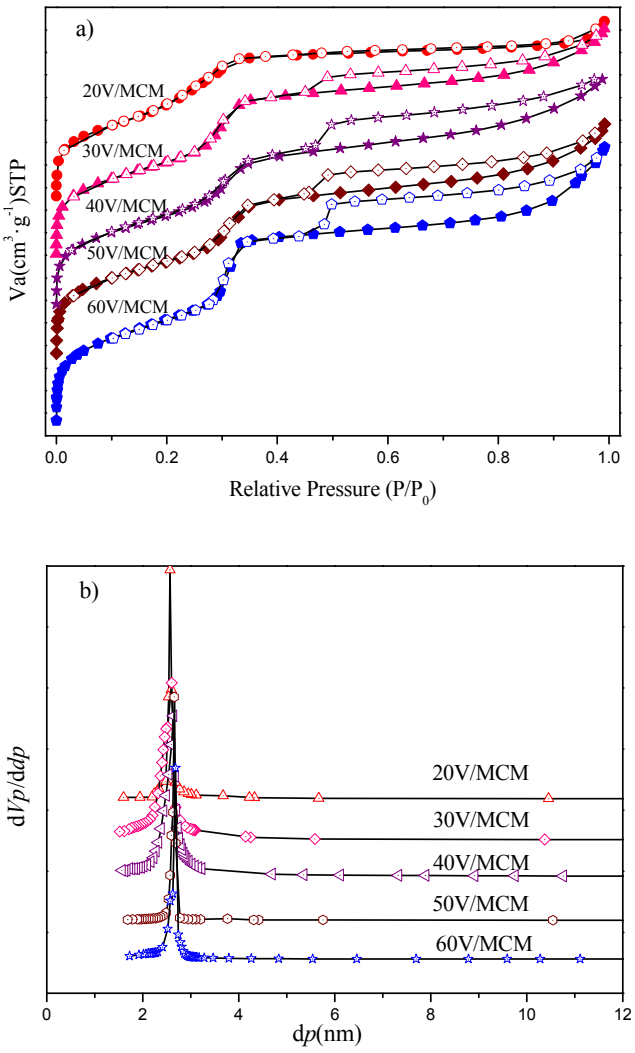

Fig. 2 N_2 adsorption/desorption isotherms (a) and pore size distribution (b) of samples containing different vanadium amounts

Table 1 Structural parameters of different vanadium samples

Samples	S_{BET} (m^2/g)	Pore volume (m^3/g)	Pore size [a] (nm)	Unit cell parameter, a_0(nm)($a_0=2xd_{100}/\sqrt{3}$)	d-spacing d_{100}(nm)	Pore wall thickness d_W(nm)($d_W=a_0-d_P$)
MCM-41 [b]	985	0.89	2.37	4.22	3.65	1.85
20V	931	0.62	2.57	4.26	3.69	1.69
30V	832	0.81	2.60	4.39	3.80	1.79
40V	831	0.80	2.63	4.49	3.89	1.86
50V	846	0.80	2.65	4.55	3.94	1.90
60V	908	0.96	2.68	4.64	4.02	1.96

[a] The most probable pore size from pore size distribution calculated by BJH method using absorption data. [b] sample represented synthesized pure MCM-41.

The morphology of samples can be confirmed by the representative SEM images of the corresponding samples, and their results were shown in Fig. 3. By comparison of sample containing different vanadium loading, obviously, the size of samples particles became smaller with increasing vanadium loading. Accordingly, the number of aggregation voids became greater. This result supported the above-mentioned N_2 adsorption analysis. We suggested that increasing loading of vanadium may influence the particles size of samples.

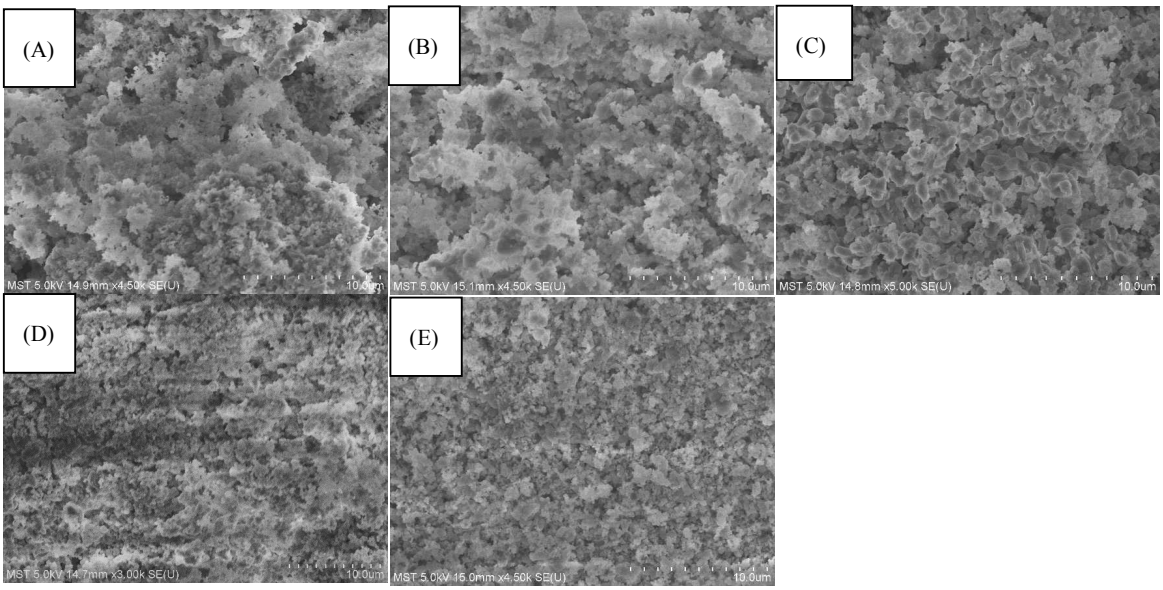

Fig .3 the SEM images of sample, (A) 20V/MCM, (B) 30V/MCM, (C) 40V/MCM, (D) 50V/MCM and (E) 60V/MCM,

In addition, more direct structural information could be obtained by TEM image of samples. The samples were tested by high-powered transmission electron microscope and elemental mapping, and the

results are shown in Fig. 4. The TEM results (Fig. 4a) demonstrated a long-range order as well as two-dimensional mesoporous structure with uniform channels, indicating that the metal oxides were embedded into the inner walls without damaging the regularity of the mesoporous phase. Also, the TEM images showed that the large metal oxide particles were invisible, and vanadium oxides may be highly dispersed in the channel of mesoporous silica due to the confinement of pore size. Besides this, element mapping analysis was used as direct evidence for the presence and distribution of vanadium oxide species. The element mapping images clearly show that the Si and O elements were uniformly and compactly distributed in the sample. While the vanadium species were dispersed uniformly in mesoporous silica, which suggested the high-dispersion of vanadia species.

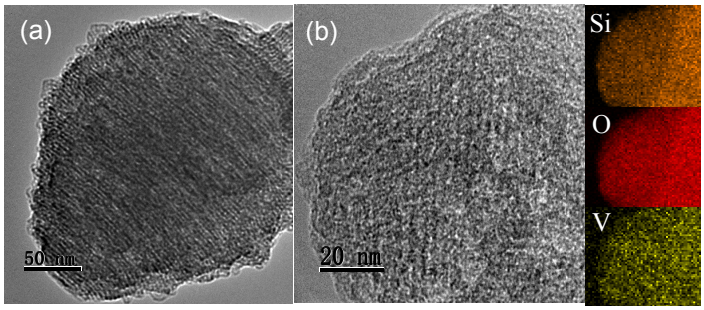

Fig. 4 TEM images (a) and elemental mapping (b) of 60V/MCM

3.2. Characterizations for the state of vanadium oxide species

High-angle XRD patterns of all the samples are shown in Fig. 5. All the curves exhibited broad diffraction peaks from 20° to 30°, which can be ascribed to amorphous silica. Another several crystal diffraction peaks located at 37°, 43°, 64° and 77° can be detected by the high-angle XRD, which can be assigned to vanadium oxide hydrate crystals ($V_2O_5.xH_2O$). It was worth noting that, when the concentration of vanadium in the composites was increased, the intensity of diffraction peaks corresponding to vanadium oxide crystals became stronger gradually, indicating aggregation and increasing crystallinity of the vanadium oxide species in the directly synthesized mesocomposites. In

addition, when compared with the directly synthesized samples, the diffraction peaks associated with the vanadium oxide crystals from the post-synthesized sample were obviously higher and sharper, indicating that the much larger crystals were formed in the wet impregnation process. This fact suggested that the less size of quantized active species could be obtained due to the confinement of narrow pore and interaction with silicate walls for vanadium species in the direct synthetic method.

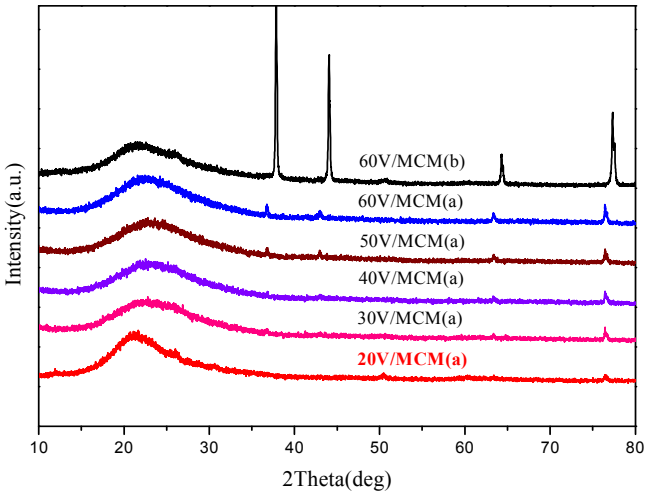

Fig. 5 High-angle XRD patterns of samples containing different vanadium amounts, a represented directly synthesized sample and b represented Post-synthesized sample.

In addition, the state of vanadium in materials were investigated with diffused reflection UV-Vis spectra. Fig. 6 shows the diffused reflection UV-vis spectra of the calcined V/MCM samples containing different vanadium amounts. All the samples showed two wide-ranges of absorption peaks at 250 nm and 410 nm, respectively, which indicating characteristic absorption of vanadium oxides. The presence of a broad band centered at ca. 250 nm was attributed to the surface isolated V^{5+} tetrahedral type VO_4^{3-} which was dispersed and interacted with the pore walls' surface.[33] This band belonged to charge transfer (CT) bands associated with V-O electron transfer $(\pi)t_2 \rightarrow (d)e$ and $(\pi)t_1 \rightarrow (d)e$. In addition, the featured peak at 410 nm shows the presence of clustered vanadium oxide species due to a further polymerization of the vanadium species,[33] reflecting that the crystallites vanadium oxides were formed

in the materials.

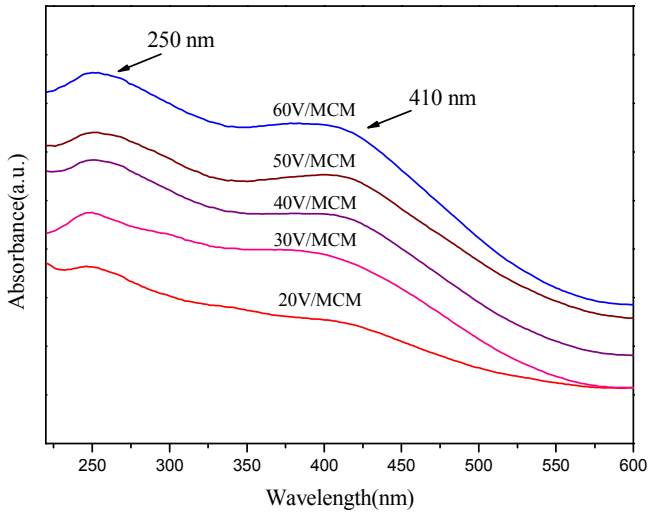

Fig. 6 Diffused reflection UV-Vis spectra from samples containing different vanadium amounts

Further precise information on the oxidation states of surface vanadium species can be obtained from XPS results. Herein, X-ray photoelectron spectroscopy of vanadium 2p region and oxygen 1s region were studied for various samples with different vanadium loadings and the V2p and O1s core-level spectra were shown in Fig. 7a and 7b, respectively. Thereinto, the core level binding energy from the $V2p_{3/2}$ and $V2p_{1/2}$ spectra were located at ca. 517.0 and 524.6 eV, respectively. The binding energy at ca. 517.0 eV was assigned to $V(5^{+})$ species in the sample, whose $V2p_{3/2}$ peak was substantially enhanced and accompanied with slight excursion to high binding energy.[34] This result was associated with the facts that VO_4^{3-} species (corresponded to a relatively low binding energy) firstly were jointed on the pore surface by bonding with silicon, and then increasing of cluster V_2O_5 (corresponded to a relatively high binding energy) in pore wall led to the excursion to high binding energy due to the decrease of electron cloud density. In Fig. 7b, the main feature peak at ca. 533.0 eV was assigned to oxygen atoms bonded to silicon. Another small peak at ca. 529 eV assigned to oxygen atoms bonded to vanadium[35] was accompanied with an ascending trend with increasing vanadium, indicating increasing numbers of vanadium oxide species on the pore walls.

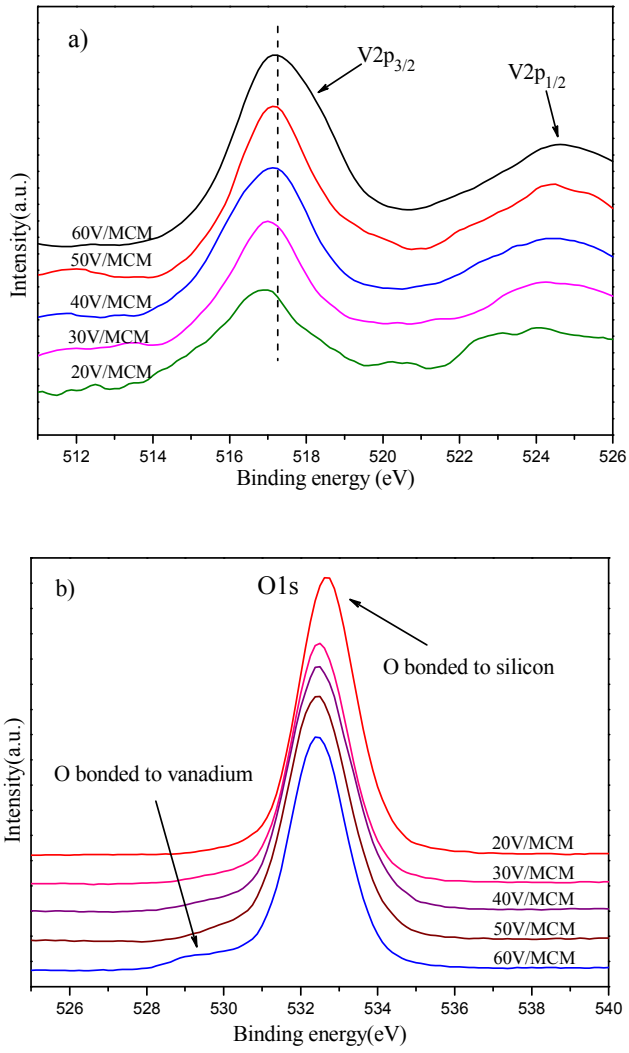

Fig. 7 X-ray photoelectron spectroscopy containing of samples different vanadium amounts, (a) V2p3/2 (smoothing) and (b) O1s.

The distribution of vanadium species on the pore walls can be reflected by the FT-IR spectra (Fig. 8). Typically, an absorption peak at 966 cm^{-1} corresponding to the stretching vibration of Si-O-H surface groups,[36, 37] became weaker with increasing vanadium concentration, implying decreased the numbers of Si-O-H on the pore walls. The observation suggested that surface Si-O-H were gradually covered with increasing vanadium oxide species. Meanwhile, the absence of surface Si-O-H may indicate that vanadium species were interacted with silicate walls. On the other hand, the FT-IR spectra of sample 30V/MCM synthesized without citrate ions, the as-synthesized uncalcined sample 30V/MCM and

sodium citrate were given for proving of citrate acid' presence. By comparison of above three samples, sample B exhibited several additional absorption peaks at 3286, 1393 and 856 cm-1 which were in accordance with citrate. In addition, additional absorption peaks presented in the sample 30V/MCM exhibited a slight shift compared with pure citrate, which can indicate the existence of interaction in the sample.

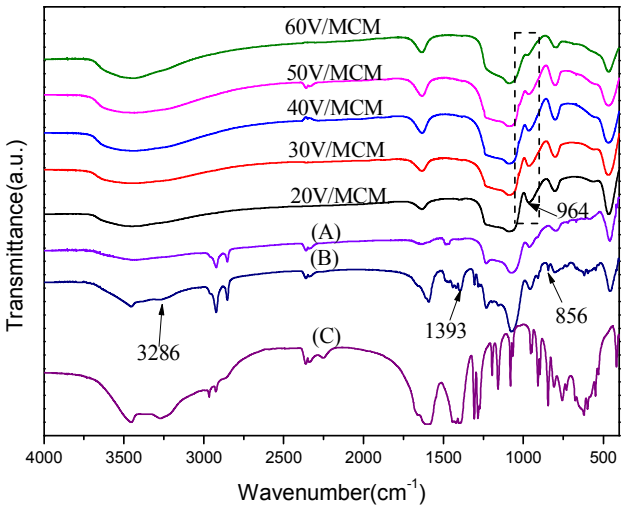

Fig. 8 FT-IR spectra of different vanadium amounts samples, (A) represented the sample 30V/MCM synthesized without citrate ions, (B) represented the as-synthesized sample 30V/MCM and (C) represented pure sodium citrate.

As known, reduction temperature is sensitive to the size of particle during reduced process. Smaller particles are expected to be reduced at lower temperature, and larger metal oxide particle size corresponds to higher reduction temperature.[27] Therefore, The H_2-TPR profiles of samples can gave more information of vanadium species state on the pore walls of mesoporous silica. The H_2-TPR patterns from the directly- and post-synthesized samples 60V/MCM are shown in Fig. 9. The results of temperature-programmed reduction are in agreement with high-angle XRD results (Fig. 1). The directly synthesized sample exhibited a sharp peak with maximum reduction temperature at T_m ca. 436 °C, whereas, the post-synthesized sample showed wider and relatively low peak with maximum reduction

temperature at T_m ca. 530 °C. The reduction temperature from the directly synthesized sample was significantly lower than that from post-synthesized sample. This result can be described by fact that the fine and uniform vanadium oxide species were highly dispersed on the pore walls of mesoporous silica due to confinement of narrow pore. As for the post-synthesized sample, high reduction temperature suggested that the large metal oxide clusters may be formed on the external surface of the mesoporous MCM-41.[33]

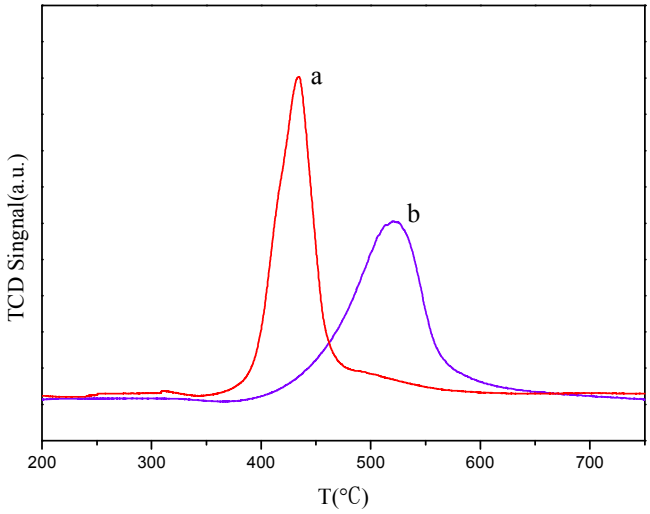

Fig. 9 H_2-TPR pattern of 60V/MCM samples (a) direct-synthesized (b) post-synthesized

3.3. Catalysis tests

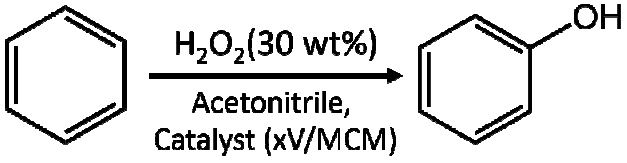

Scheme 2. the synthesis of phenol by direct oxide of benzene

In order to evaluate the catalytic properties of the series of V/MCM samples containing different vanadium contents, the direct oxidation of benzene was selected as a probe reaction. The corresponding catalytic results were summarized in Table 2. The tested results exhibited an ascending conversions of the benzene with increasing vanadium content in the samples. This result was apparently associated with increasing more accessible active sites on the surface of the catalyst, due to increasing coverage of

vanadium oxide species on the MCM-41 pore walls. While the V/Si molar ratio in material was up to 10.06 %, conversions of benzene were not significantly improved. We suggested that the surface coverage of vanadium oxides on the pore walls had been nearly saturated, which was in agreement with the FT-IR results. On the other hand, the directly synthesized sample 60V/MCM exhibited higher catalytic activities, when compared with that from the corresponding post-synthesized sample 60V/MCM (P) and 60V/MCM (N). In addition, when the maximum vanadium amount was added into post synthesized process of sample 60V/MCM (N), but corresponding high-loading of vanadium was not obtained for the sample synthesized without citrate. Meanwhile, compared with directly synthesized sample 40V/MCM, we found that the sample 60V/MCM (N) did not give more conversion of benzene even with higher vanadium loading. The result may be ascribed to that metal atoms were incorporated in the framework of mesoporous silica, and exposed active sites should be fewer than that of in the directly synthesized sample. Finally, pure V_2O_5 crystal was used as catalyst to catalyze oxidation of benzene and exhibited relatively low activities. This result indicated that the bulk V_2O_5 crystal possessed few catalytic active sites, while highly-dispersed vanadium (5+) species can efficiently catalyze the reaction. Herein, based on the above characterizations, we believed that highly-dispersed and high-loading catalytic active centers were produced in situ on the surface of pore walls by the directed synthesis method, and its number was significantly higher than that of post-synthesized. Therefore, the catalytic result also in favor of the proposed templating synthesized methods.

In addition, recycling test results from the directly- and post-synthesized samples in the benzene hydroxylation are shown in Table 3. The post-synthesized sample did not exhibit reusability in the reaction, while the catalytic activity from the directly synthesized samples deteriorated slowly in comparison with that from the post-synthesized samples. We can thus conclude that the vanadium oxide species from the directly synthesized sample exhibited stronger interaction with the pore walls of the

mesoporous silica, leading to more stable active centers in the catalyst. On the other hand, results from N_2 adsorption/desorption showed gradually increasing pore wall thickness for the series of directly synthesized samples, which may be another reason for the higher stability of catalyst due to that high vanadium species surface coverage on the pore walls decreased contact between the silicate walls and water in the reaction system.

Table 2 Catalytic properties of samples in the hydroxylation of benzene [a]

Sample	V/Si (%) [b]	Benzene conversion (%)	Phenol selectivity (%)
20V/MCM	3.74	14.3	88
30V/MCM	6.01	20.1	89
40V/MCM	8.42	25.4	87
50V/MCM	10.06	28.2	89
60V/MCM	11.13	29.1	90
60V/MCM(P) [c]	11.17	12.3	89
60V/MCM(N) [d]	8.13	18.3	93
V_2O_5	-	4.4	78

[a] Reaction conditions: catalyst amount 0.1 g, benzene 2 ml, CH_3CN 15 ml, 30% H_2O_2 6.89 ml, temperature 30°C and duration 10 h. [b] V/Si molar ratios were analyzed by ICP. [c] Post-synthesized sample. [d] the sample was synthesized according to direct method without adding citrate.

Table 3 Recycling property of directly- and post-synthesized catalyst [a]

Samples	Runs	V/Si (%) [b]	Benzene conversion (%)	Phenol selectivity (%)
direct-60V/MCM	1	11.13	29.1	90
	2	8.13	23.2	89
	3	3.43	15.1	87
	4	1.45	8.3	89
post-60V/MCM	1	11.17	12.3	89
	2	2.11	6.1	94
	3	0.12	trace	-

[a] Reaction conditions described as above, directly- and post-synthesized samples contain identical vanadium amount. [b] V/Si molar ratios were analyzed by ICP.

4. Conclusions

In summary, surface functional mesoporous silica encapsulating vanadium oxide species was prepared successfully via direct templating assemble route. The surface functionalization of silicate wall was closely associated with metallization of micelle. The vanadium oxide species on the pore walls exhibited a high-dispersion and gradual coverage on the silicate surface with increasing vanadium concentration in samples. The direct synthetic catalysts showed special catalytic activities in comparison with post-synthesized samples from benzene hydroxylation. This direct synthesis can potentially be utilized to prepare mesoporous materials containing other metal oxides and transition metal nanoparticles by modifying micelles template. These composite materials have potentially extensive applications in catalysis.

Acknowledgements

The authors acknowledge the financial support of the National Natural Science Foundations of China (21276125, 20876077 and 21476108).

Notes and references

1 C. T. Kresge, M. E. Leonowicz, W. J. Roth, J. C. Vartuli and J. S. Beck, *Nature*, **1992**, 359, 710-712.

2 J. S. Beck, J. C. Vartuli, W. J. Roth, M. E. Leonowicz, C. T. Kresge, K. D. Schmitt, C. T. W. Chu, D. H. Olson, E. W. Sheppard, S. B. McCullen, J. B. Higgins and J. L. Schlenker, *J. Am. Chem. Soc.*, **1992**, 114, 10834-10843.

3 A. Corma, *Chem. Rev.*, **1997**, 97, 2373-2419.

4 K. Schumacher, C. D. von Hohenesche, K. K. Unger, R. Ulrich, A. Du Chesne, U. Wiesner and H. W. Spiess, *Adv. Mater.*, **1999**, 11, 1194-1198.

5 Y. Han, F. S. Xiao, S. Wu, Y. Y. Sun, X. J. Meng, D. S. Li, S. Lin, F. Deng and X. J. Ai, *J. Phys. Chem. B*, **2001**, 105, 7963-7966.

6 B. Han, H. Wang, Y. Kong and J. Wang, *Mater. Lett.*, **2013**, 100, 159-162.

7 C. Wu, Y. Kong, F. Gao, Y. Wu, Y. Lu, J. Wang and L. Dong, *Microporous and Mesoporous Mater.*, **2008**, 113, 163-170.

8 E. J. Acosta, C. S. Carr, E. E. Simanek and D. F. Shantz, *Adv. Mater.*, **2004**, 16, 985-+.

9 M. Alvaro, M. Benitez, D. Das, B. Ferrer and H. Garcia, *Chem. Mater.* , **2004**, 16, 2222-2228.

10 M. Alvaro, A. Corma, D. Das, V. Fornes and H. Garcia, *Chem. Commun.*, **2004**, 956-957.

11 M. Alvaro, B. Ferrer, H. Garcia and F. Rey, *Chem. Commun.*, **2002**, 2012-2013.

12 K. Ariga, *Chem. Rec.*, **2004**, 3, 297-307.

13 A. Liberman, N. Mendez, W. C. Trogler and A. C. Kummel, *Surf. Sci. Rep.*, **2014**, 69, 132-158.

14 P. Xu, X. Li, H. Yu and T. Xu, *Sensors*, **2014**, 14, 19023-19056.

15 Z. Li, J. C. Barnes, A. Bosoy, J. F. Stoddart and J. I. Zink, *Chem. Soc. Rev.*, **2012**, 41, 2590-2605.

16 R. Metivier, I. Leray, B. Lebeau and B. Valeur, *J. Mater. Chem.*, **2005**, 15, 2965-2973.

17 M. Mandal, V. Nagaraju, B. Sarma, G. V. Karunakar and K. K. Bania, *Chempluschem*, **2015**, 80, 749-761.

18 R. Zubrzycki, J. D. Epping and T. Ressler, *Chemcatchem*, **2015**, 7, 1112-1121.

19 H. Wang, W. Qian, J. Chen, Y. Wu, X. Xu, J. Wang and Y. Kong, *Rsc. Adv.*, **2014**, 4, 50832-50839.

20 I. E. Wachs, *Dalton. T.*, **2013**, 42, 11762-11769.

21 N. A. Melosh, P. Lipic, F. S. Bates, F. Wudl, G. D. Stucky, G. H. Fredrickson and B. F. Chmelka, *Macromolecules*, **1999**, 32, 4332-4342.

22 H. Miyata, T. Noma, M. Watanabe and K. Kuroda, *Chem. Mater.*, **2002**, 14, 766-772.

23 B. J. Scott, G. Wirnsberger and G. D. Stucky, *Chem. Mater.*, **2001**, 13, 3140-3150.

24 M. Templin, A. Franck, A. DuChesne, H. Leist, Y. M. Zhang, R. Ulrich, V. Schadler and U. Wiesner, *Science*, **1997**, 278, 1795-1798.

25 T. C. Xiao, S. F. Ji, H. T. Wang, K. S. Coleman and M. L. H. Green, *J. Mol. Catal., A-Chem.*, **2001**, 175, 111-123.

26 H. F. Yang, Q. H. Shi, X. Y. Liu, S. H. Xie, D. C. Jiang, F. Q. Zhang, C. Z. Yu, B. Tu and D. Y. Zhao, *Chem. Commun.*, **2002**, 2842-2843.

27 C. Huo, J. Ouyang and H. Yang, *Sci. Rep-UK.*, **2014**, 4.

28 K. Niu, L. Liang, H. Geng, W. Hou, H. Tian and S. Liu, *Mater. Lett.*, **2013**, 107, 325-328.

29 K. Niu, L. Liang, Y. Gu, L. Ke, F. Duan and M. Chen, *Langmuir*, **2011**, 27, 13820-13827.

30 K. Niu, D. Shi, W. Dong, M. Chen and Z. Ni, *J. Colloid Interf. Sci.*, **2011**, 362, 74-80.

31 H. F. Yang, Q. Y. Lu, F. Gao, Q. H. Shi, Y. Yan, F. Q. Zhang, S. H. Xie, B. Tu and D. Y. Zhao, *Adv. Funct. Mater.*, **2005**, 15, 1377-1384.

32 W. H. Zhang, M. Froba, J. L. Wang, P. T. Tanev, J. Wong and T. J. Pinnavaia, *J. Am. Chem. Soc.*, **1996**, 118, 9164-9171.

33 B. Solsona, T. Blasco, J. M. L. Nieto, M. L. Pena, F. Rey and A. Vidal-Moya, *J. Catal.*, **2001**, 203, 443-452.

34 H. Choi, J.-H. Bae, D. H. Kim, Y.-K. Park and J.-K. Jeon, *Materials*, **2013**, 6, 1718-1729.

35 J. George, S. Shylesh and A. P. Singh, *Appl. Catal., A-Gen.*, **2005**, 290, 148-158.

36 E. Caponetti, A. Minoja, M. L. Saladino and A. Spinella, *Microporous and Mesoporous Mater.*, **2008**, 113, 490-498.

37 B. L. Su, A. Leonard and Z. Y. Yuan, *CR. Chim.*, **2005**, 8, 713-726.